25th IMEKO TC4 International Symposium
23rd International Workshop on ADC and DAC Modelling and Testing
IMEKO TC-4 2022
Brescia, Italy / September 12-14, 2022

First results on the functional characterization of two rotary comb-drive actuated MEMS microgripper with different geometry

Gabriele Bocchetta[1], Giorgia Fiori[2], Andrea Scorza[3], Nicola Pio Belfiore[4], Salvatore Andrea Sciuto[5]

Dep. of Industrial, Electronic and Mechanical Engineering, Roma TRE University, Rome, Italy
[1] gabriele.bocchetta@uniroma3.it, [2] giorgia.fiori@uniroma3.it, [3] andrea.scorza@uniroma3.it,
[4] nicolapio.belfiore@uniroma3.it, [5] salvatore.sciuto@uniroma3.it

***Abstract* – Microgrippers (MGs) are Micro Electro-Mechanical System (MEMS) devices able to manipulate cells and micrometric objects. In order to carry out their functional characterization, a comparison between two electrostatic rotary comb-drives actuated prototypes with different geometries through an image analysis-based method is proposed. This study aims at evaluating and comparing the MGs displacement as a function of the supply voltage. The two investigated geometries are equipped with a single rotary comb-drive and a double rotary comb-drive actuation. MGs data have been collected through a trinocular optical microscope with a digital camera and processed by means of an algorithm implemented *ad hoc* in MATLAB. Based on the promising results obtained, further studies are going to be carried out by including other geometries and improving the experimental setup and implemented method.**

I. INTRODUCTION

Microgrippers (MGs) are devices that are part of the class of MEMS (Micro Electro-Mechanical System) devices. These devices require micro-actuators to move the gripper jaws, thus offering a wide range of possible applications, especially in the biomedical sector [1-3]. In literature, there are studies on different types of micro-actuators, based on different operating principles, i.e., electrostatic, electromagnetic, electrothermal, piezoelectric, and shape memory alloys [4-6]. The MG prototypes under examination are equipped with electrostatic rotary comb-drives and Conjugate Surface Flexure Hinges (CSFHs) and fabricated monolithically on a Silicon-on-Insulator (SOI) wafer with an aluminum hard mask, through a process of Deep Reactive Ion Etching (DRIE) [9-10]. Previous studies available in literature [11-12] have presented a theoretical formulation describing the electrostatic torque exerted by rotary comb-drives, which is a function of the geometric characteristics of the micro-actuator, whose nominal values have been reported in Table 1, and the square of the supply voltage and have evaluated the displacement as a function of the latter [13-15]. This preliminary study, based on image analysis method, aims to investigate the design of MG prototypes by analyzing the relationship between gripper tips displacement and the number of active micro-actuators, as a function of supply voltage and to verify if doubling the electrostatic torque applied by the comb-drives, the prototype displacements double, as assumed by the theoretical model [9-12]. In particular, the two Devices Under Test (DUTs) are two new-concept MG prototypes composed of a double four-bar linkage in a mirroring configuration actuated by electrostatic rotary comb-drives. The main difference between the two investigated geometries is the comb-drive number: the first prototype (Fig. 1a) is actuated by a Single Rotary Comb-Drive (SRCD), while the second one (Fig. 1b) by a Double Rotary Comb-Drive (DRCD).

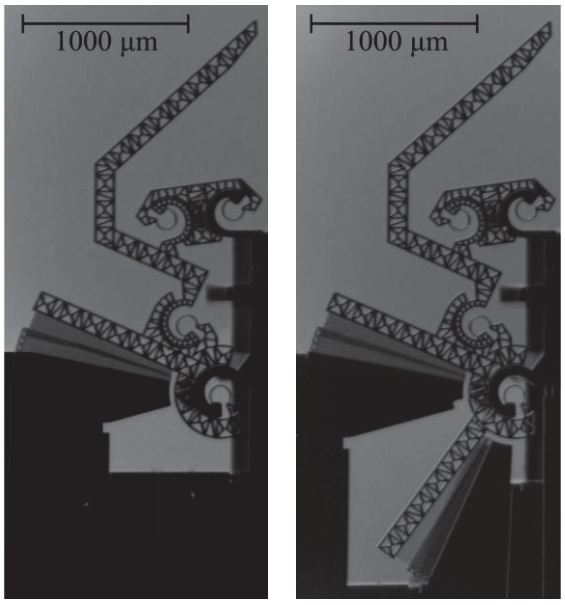

(a) (b)

Fig. 1. Geometry comparison between (a) single and (b) double rotary comb-drive actuated microgripper.

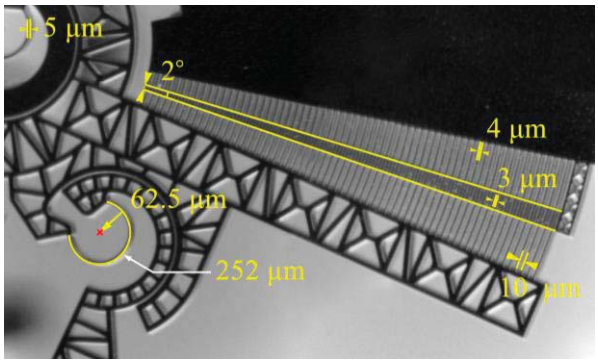

Fig. 2. Microgripper geometric characteristics.

Table 1. Microgripper main specifications

Component		SRCD	DRCD
Number of comb-drives		2	4
Fingers	Number per comb-drive	64	
	Width	4 µm	
	Thickness	40 µm	
	Distance	10 µm	
	Initial overlapping angle	2°	
	Rotor-stator distance	3 µm	
CSFH	Number	8	
	Curved beam length	252 µm	
	Curved beam width	5 µm	
	Curved beam thickness	40 µm	
	Curvature radius	62.5 µm	
SOI Wafer	Device layer thickness	40 µm	
	Insulated layer thickness	5 µm	
	Handle layer thickness	400 µm	

II. MATERIALS AND METHODS

In order to evaluate the functional characteristics of the two DUTs, different videos have been acquired using a trinocular optical microscope equipped with a digital camera and the corresponding data have been processed by a measurement procedure implemented by the Authors in MATLAB. In particular, some videos of the MG jaws and the comb-drive that the two prototype geometries have in common (Fig. 2) have been acquired, for the purpose of evaluating the MG displacement. The two DUTs have been powered by an Arbitrary/Function Generator that supplied a trapezoidal ramp signal, in order to assess the displacement as the supply voltage increases.

A. Experimental setup

The experimental setup is shown in Fig. 3, while its main components have been reported in Table 2, and can be schematized considering two main parts:

- Power supply system, consisting of an Arbitrary /Function Generator and a power amplifier for the MG prototypes supply signal generation.
- Image acquisition system, consisting of a trinocular optical microscope and a digital camera for acquiring videos of the DUTs.

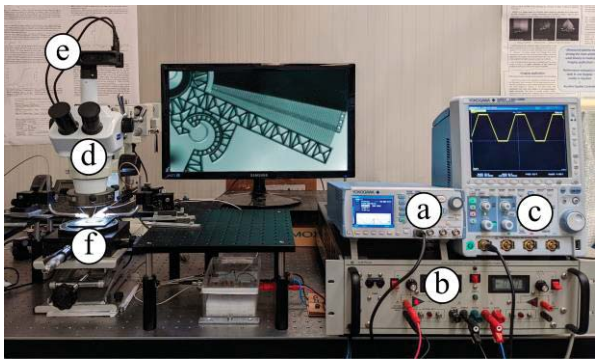

Fig. 3. Experimental setup: (a) Arbitrary/Function Generator, (b) Power Amplifier, (c) Oscilloscope, (d) Light Microscope, (e) Digital Camera, and (f) DUT.

The MG prototypes have been placed under the microscope lens and have been powered through the contact of three tungsten needles, positioned by three micropositioners. The Arbitrary/Function Generator has been configured to generate a trapezoidal ramp signal with a 2 s period, thus obtaining for each period a phase with a duration of 0.5 s corresponding to the maximum supply voltage. The generated signal subsequently has been amplified, thus obtaining a supply voltage between 0 e 20 V peak-to-peak and a digital oscilloscope (Fig. 3c) has been placed in parallel with the supply circuit in order to monitor in real-time the supply voltage powering the DUT. Different videos of the DUTs have been acquired using the microscope-mounted digital camera at a frame rate of 60 fps, and with a duration to capture at least thirty periods of the supply signal and thirty frames for each period showing the MG at the maximum displacement. In particular, videos of the

Table 2. Experimental Setup

Device	Characteristics
Arbitrary/ Function Generator	Amplitude: 0 to ± 10 V peak-to-peak, Frequency: 0.01 µHz to 5 MHz
Power Amplifier	Amplitude: 0 to ± 20 V
Light Microscope	Zoom Range: 16×, 20×, 40×, 60×, 80×, 100×
Light source	LED Ring Light Color temperature: 5600 °K
Digital Camera	23.3 MP, sensor size ½.3 in, maximum image size 5568×4176 pixel
Image Processing Software	In-house algorithm implemented in MATLAB (2021b, MathWorks)
PC	Intel core i7-4790, 32 GB RAM, Nvidia GeForce GTX 960

comb-drive at 40× magnification and videos of the MG jaws at 80× magnification have been acquired for evaluating the angular displacement of the micro-actuators and the gripper tips displacement respectively.

B. Video processing

The collected data have been processed in a MATLAB environment. The comb-drive angular displacement and the gripper tip displacement have been evaluated through a measurement procedure that performs a tracking of virtual markers inserted frame by frame within predetermined Regions Of Interest (ROIs) as shown in Fig. 4 [15-18]. As regards the comb-drive videos, the Instantaneous Center of Rotation (ICR) of the comb-drive has been obtained on the first frame from the intersection of two lines drawn by the operator, and the angular displacement has been evaluated as follows:

$$\vartheta = \frac{s}{r} \tag{1}$$

where ϑ describes the angular displacement made by the comb-drive, that it has been evaluated as the ratio between the markers trajectory which describes an arc of a circle s, and the radius r, calculated as the distance between the ICR and markers x- and y-coordinates. Finally, the comb-drive average angular displacement and the gripper tip displacement have been evaluated as the mean over all acquired periods.

Table 3. Main uncertainty sources

Source	Value
Arbitrary/Function Generator amplitude uncertainty	±(1% of $V_{peak\text{-}to\text{-}peak}$ + 2 mV)
Arbitrary/Function Generator frequency uncertainty	±(3 ppm of setting + 2 pHz) Aging rate: ±1 ppm/year
Power amplifier amplitude uncertainty	2 mV
Optical system uncertainty	1 µm
Video tracking algorithm uncertainty	It depends on the subject of the video and magnification level. It has been estimated as 0.01° for comb-drive videos and 0.1 µm for SRCD gripper tip videos and 0.3 µm for DRCD gripper tip videos respectively

III. UNCERTAINTY ANALYSIS

In order to discuss the obtained results, an uncertainty analysis considering the main sources of uncertainty has been carried out. In according with the approach adopted in [13-15], Type A and Type B uncertainties have been combined [19], following:

$$\sigma_T = \sqrt{\sigma_A^{\,2} + \sigma_B^{\,2}} \tag{2}$$

Type A uncertainties σ_A have been evaluated considering the standard deviation of the obtained results, while Type B uncertainties σ_B have been calculated by taking into consideration the following sources of uncertainty present in the measurement chain, listed in Table 3:

- Arbitrary/Function Generator on signal amplitude and frequency, reported in the datasheet.
- Power amplifier uncertainty on amplitude, reported in the datasheet.
- Optical system uncertainty has been overall estimated as 1 µm. This contribution considers the lateral resolution that depends on diffraction and the wavelength of the incident light, and the pixel resolution [20-22].
- Video tracking algorithm uncertainty, which varies frame by frame and depends on the type of considered video, i.e., comb-drive or gripper tip.

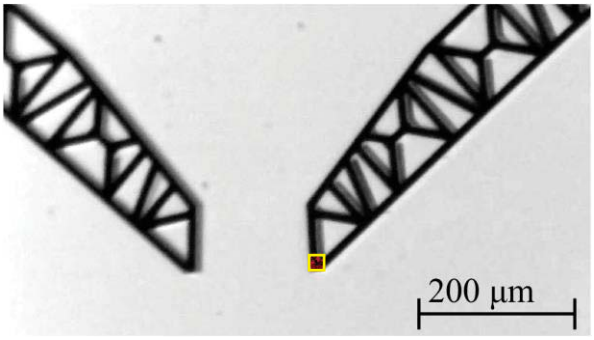

Fig. 4. Virtual marker (red) inserted in the ROI (yellow) for motion evaluation through video tracking.

Table 4. Variable settings in MCS

Data	Parameter	Distribution	
Comb-drive videos	ICR x-coordinate	Normal	x_{ICR} ± 5 px
	ICR y-coordinate	Normal	y_{ICR} ± 1 px
	MC x-coordinate	Normal	x_{MC} ± 2 px
	MC y-coordinate	Normal	y_{MC} ± 2 px
Gripper tip videos	MC x-coordinate	Normal	x_{MC} ± 2 px
	MC y-coordinate	Normal	y_{MC} ± 2 px

x_{ICR}, y_{ICR}, x_{MC} and y_{MC} indicate the ICR and MC average x- and y-coordinates which depend on the video of each investigated device due to a different frame during the acquisition.

The video tracking algorithm uncertainty has been evaluated by the means of a Monte Carlo Simulation (MCS) with 10^4 iterations [23]. At each MCS iteration, the number of markers inserted in the ROI has been made to vary randomly, thus obtaining a variation of the Markers' Centroid (MC) x- and y-coordinates. Concerning the comb-drive angular displacement evaluation, since the implemented algorithm requires a manual step for the ICR assessment, its contribution in

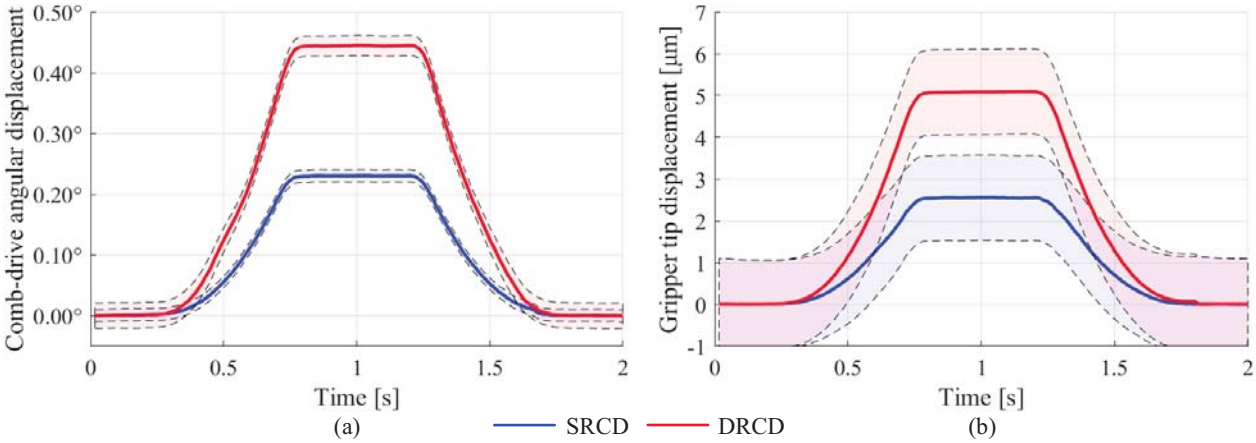

Fig. 5. SRCD and DRCD results: (a) comb-drive angular displacement and (b) gripper tip displacement as a function of the supply voltage.

the uncertainty analysis has been evaluated by varying the ICR coordinates according to the distribution obtained after performing the ICR evaluation process by six different operators, 30 times each. Finally, the evaluated uncertainties have been expressed as the overall calculated standard deviations and have been combined for reporting the measured results referring to a single average period.

Table 5. Experimental results

	SRCD	**DRCD**
Comb-drive angular displacement	0.23° ± 0.01°	0.45° ± 0.02°
Gripper tip displacement	2.5 ± 1.1 µm	5.1 ± 1.1 µm

IV. RESULTS AND DISCUSSION

In this section, the first obtained results correlated by the relative uncertainties are reported and commented. Fig. 5 shows the comb-drive angular displacements and the gripper tip displacement together with their total uncertainties obtained applying to the two MGs a power supply in the range 0-20 V peak-to-peak. The obtained preliminary results reported in Table 5 show that the maximum angular displacement corresponds to 0.23° ± 0.01° and 0.45° ± 0.02° for SRCD and DRCD respectively, while the gripping tip maximum displacement is 2.5 ± 1.1 µm for SRCD and 5.1 ± 1.1 µm for DRCD. Therefore, considering the stationary part of the curves, due to the maximum supply voltage, the average ratio between DRCD and SRCD displacement is very close to 2, i.e., 1.93 ± 0.06 for the comb-drive angular displacement and 2.0 ± 0.4 for the gripper tip displacement.

V. CONCLUSIONS

The present preliminary study focused on the functional characterization of two MG prototypes with different geometry actuated by electrostatic rotary comb-drives. The two investigated devices are made up of a double four-bar linkage in a symmetrical configuration and respectively equipped with SRCD and DRCD micro-actuators. In order to evaluate the prototypes functional characteristics, videos of the two DUTs have been acquired using a trinocular optical microscope equipped with a digital camera. The acquired data have been processed through an in-house algorithm implemented in MATLAB by the authors and the uncertainty analysis has been carried out in order to estimate the quality of the measurements. For the two examined devices, the maximum angular displacement, i.e., at 20 V supply voltage, is 0.23° ± 0.01° for SRCD and 0.45° ± 0.02° for DRCD with a ratio of 1.93 ± 0.06. On the other hand, the maximum gripper tip displacement corresponds to 2.5 ± 1.1 µm and 5.1 ± 1.1 µm for SRCD and DRCD respectively, with a ratio of 2.0 ± 0.4. These preliminary results show that, as a first attempt, duplicating the number of the active micro-actuators reflects in MG double displacements.

In the near future, it will be important to improve the experimental setup and the video processing algorithm and to investigate other MG geometries with the aim to assess if the CSFHs behavior can be assumed linear as a function of the supply voltage, within the considered range of displacements, and moreover, to investigate if different microactuator geometries also correspond to different values of the pull-in voltage [24].

REFERENCES

[1] D.O.Otuya, Y.Verma, H.Farrokhi, L.Higgins, M.Rosenberg, C.Damman, G.J.Tearney, "Non-endoscopic biopsy techniques: a review", Expert Rev Gastroenterol Hepatol, vol.12, No.2, February 2018, pp. 109-117.

[2] A.Bagolini, P.Bellutti, P.Di Giamberardino, I.J.Rudas, V.D'Andrea, M.Verotti, A.Dochshanov, N.P.Belfiore, "Stiffness characterization of biological tissues by means of MEMS-technology

based micro grippers under position control", Mech. Mach. Sci., July 2017, pp. 939–947.

[3] K.R.Oldham, "Applications of MEMS technologies for minimally invasive medical procedures", in "MEMS for Biomedical Applications", Woodhead Publishing, 2012, pp. 269-290.

[4] P.K.Sekhar, V.Uwizeye, "Review of sensor and actuator mechanisms for bioMEMS", in "MEMS for Biomedical Applications", Woodhead Publishing, 2012, pp. 46-77.

[5] S.Yang, Q.Xu, "A review on actuation and sensing techniques for MEMS-based microgrippers", J Micro-Bio Robot, vol.13,No.1, May 2017,pp. 1-14.

[6] H.Llewellyn-Evans, C.A.Griffiths, A.Fahmy, "Microgripper design and evaluation for automated μ-wire assembly: a survey". Microsystem Technologies, vol.26, No. 6, January 2020, pp. 1745-1768.

[7] N.P.Belfiore, A.Bagolini, A.Rossi, G.Bocchetta, F.Vurchio, R.Crescenzi, A.Scorza, P.Bellutti, S.A.Sciuto, "Design, Fabrication, Testing and Simulation of a Rotary Double Comb Drives Actuated Microgripper", Micromachines, vol.12, No.10, October 2021, p. 1263.

[8] A.Bagolini, S.Ronchin, P.Bellutti, M.Chistè, M.Verotti, N.P.Belfiore, "Fabrication of Novel MEMS Microgrippers by Deep Reactive Ion Etching with Metal Hard Mask", J. Microelectromechanical Syst., vol.26, No.4, May 2017, pp. 926-934.

[9] J.Andrew Yeh, J.-Y.Huang, C.-N.Chen, C.-Y.Hui, "Design of an electrostatic rotary comb actuator", Journal of Micro/Nanolithography, MEMS, and MOEMS, vol.5, No.2, April 2006, 023008.

[10] N.P.Belfiore, G.B.Broggiato, M.Verotti, R.Crescenzi, M.Balucani, A.Bagolini, P.Bellutti, M.Boscardin, "Development of a MEMS technology CSFH based microgripper," Proc. of 23rd International Conference on Robotics in Alpe-Adria-Danube Region, IEEE RAAD, January 2014, pp. 1-8.

[11] H.Chang, H.Zhao, F.Ye, et al., "A rotary comb-actuated microgripper with a large displacement range", Microsystem Technologies, vol.20, No.1, January 2014. pp. 119-126.

[12] L.A.Velosa-Moncada, L.A.Aguilera-Cortés, M.A.González-Palacios, J.P.Raskin, A.L.Herrera-May, "Design of a Novel MEMS Microgripper with Rotatory Electrostatic Comb-Drive Actuators for Biomedical Applications", Sensors, vol.18, No. 5, May 2018, p. 1664.

[13] F.Vurchio, G.Fiori, A.Scorza, S.A.Sciuto, "A comparison among three different image analysis methods for the displacement measurement in a novel MEMS device," Proc. of 24th IMEKO TC4 International Symposium and 22nd International Workshop on ADC and DAC Modelling and Testing, 2020, pp. 327–331.

[14] F.Vurchio, G.Fiori, A.Scorza, S.A.Sciuto, "Comparative evaluation of three image analysis methods for angular displacement measurement in a MEMS microgripper prototype: a preliminary study", ACTA IMEKO, vol.10, No.2, June 2021, pp.119-125.

[15] F.Vurchio, G.Bocchetta, G.Fiori, A.Scorza, N.P.Belfiore, S.A.Sciuto, "A preliminary study on the dynamic characterization of a MEMS microgripper for biomedical applications," Proc. of 2021 IEEE International Symposium on Medical Measurements and Applications (MeMeA), 2021.

[16] J.Shi, C.Tomasi, "Good Features to Track," Proc. of the IEEE Conference on Computer Vision and Pattern Recognition, June 1994, pp. 593–600.

[17] C.Tomasi, T.Kanade, "Detection and Tracking of Point Features", Carnegie Mellon University Technical Report CMU-CS-91-132, April 1991.

[18] Z.Kalal, K.Mikolajczyk, J.Matas, "Forward-Backward Error: Automatic Detection of Tracking Failures," Proc. of the 20th International Conference on Pattern Recognition, August 2010, pp. 2756–2759.

[19] ISO/IEC. Part 3: guide to the expression of uncertainty in measurement (GUM:1995). In Guide 98-3: 2008, Uncertainty of Measurement; ISO/IEC: Geneva, Switzerland, 2008.

[20] P.Prasad, "Introduction to Biophotonics", John Wiley and Sons, Inc, 2003.

[21] X.Heng, D.Erickson, L.R.Baugh, Z.Yaqoob, P.W.Sternberg, D.Psaltis, C.Yang, "Optofluidic microscopy–a method for implementing a high resolution optical microscope on a chip", Lab Chip, vol.6, No.10, October 2006, pp. 1274–1276.

[22] D.S.Zhang, et al., "Displacement/strain measurements using an optical microscope and digital image correlation", Optical Engineering, vol.45, No.3, March 2006, 033605.

[23] G.Fiori, A.Scorza, M.Schmid, J.Galo, S.Conforto, S.A.Sciuto, "A novel method for the gain conversion factor estimation in quality assessment of ultrasound diagnostic systems," Proc. of 2022 IEEE International Symposium on Medical Measurements and Applications (MeMeA), 2022, "in press".

[24] K.Ramakrishnan, H.Srinivasan, "Closed form models for pull-in voltage of electrostatically actuated cantilever beams and comparative analysis of cantilevers and microgripper", Journal of Electrical Engineering, vol.63, No.4, July 2012, pp. 242-248.